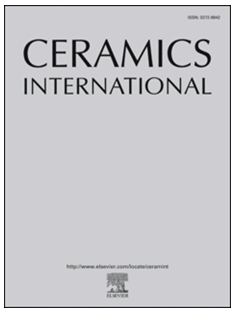

Modeling optical amplification in Er/Yb-codoped integrated Bragg gratings

Ángel Sanz-Felipe, Rocío Ariza, David Benedicto, Manuel Macias-Montero, Juan A. Vallés, Javier Solís

PII: S0272-8842(23)01792-3

DOI: https://doi.org/10.1016/j.ceramint.2023.06.206

Reference: CERI 37028

To appear in: *Ceramics International*

Received Date: 30 March 2023

Revised Date: 31 May 2023

Accepted Date: 20 June 2023

Please cite this article as: Á. Sanz-Felipe, Rocí. Ariza, D. Benedicto, M. Macias-Montero, J.A. Vallés, J. Solís, Modeling optical amplification in Er/Yb-codoped integrated Bragg gratings, *Ceramics International* (2023), doi: https://doi.org/10.1016/j.ceramint.2023.06.206.

Photoluminescence in Rare Earths: Photonic Materials, PRE'22-Poland (satellite symposium)

Modeling optical amplification in Er/Yb-codoped integrated Bragg gratings

Ángel Sanz-Felipe[1], Rocío Ariza[2], David Benedicto[3], Manuel Macias-Montero[2], Juan A. Vallés[3], and Javier Solís[2]

[1] Centro Universitario de la Defensa (CUD-AGM), Ctra. de Huesca s/n, Zaragoza 50090, Spain, angel_sf@unizar.es
[2] Grupo de Procesado por Láser, Instituto de Óptica "Daza de Valdés" (IO, CSIC), Serrano 121, Madrid 28006, Spain
[3] Dpto. de Física Aplicada & I3A, Universidad de Zaragoza, C/ Pedro Cerbuna 12, Zaragoza 50009 Spain

ABSTRACT

Bragg gratings inscribed in active waveguides combine very efficient reflective properties with the amplifying capability of rare-earths, which may lead to large amplification and lasing performance. However, the response of these photonic structures highly depends on the grating parameters and working conditions, so modeling their behavior and dependences becomes fundamental. In this work, a numerical method has been implemented to simulate the optical power propagation along an Er/Yb-codoped integrated waveguide Bragg grating as a function of its most relevant operational parameters. The results obtained show the optimal conditions to maximize its performance as a highly amplifying reflector, but also its capability as a monolithic laser. In addition, the modeling results adequately match experimental values measured in fs-laser written structures in Er/Yb-codoped phosphate glass, supporting the accuracy of the numerical method developed and its usefulness for further optimizing these promising photonic structures.

KEYWORDS: Active waveguide; Integrated Bragg grating; Amplified reflector; Monolithic laser

1. INTRODUCTION

Active waveguide Bragg gratings (AWBG) consist of a periodic perturbation of the refractive index inside rare-earth doped waveguides. The Bragg grating (BG) produces an efficient reflection of a light wave at some particular wavelengths that satisfy the Bragg condition [1,2]. This behavior leads to several current and potential photonic applications and devices in integrated optics, signal filtering, physical and chemical sensing, and mirrors for laser cavities [2–7]. On the other hand, the active character of the rare-earth doped material may lead to light amplification that can overcome the propagation losses so that a power gain can be obtained [8–10]. Therefore, the combination of both behaviors in such structures leads to promising photonic applications such as monolithic lasing and amplifying reflectors [11–14].

The BG and AWBG fabrication procedure by means of ultrafast laser pulses has been intensively developed and improved over the last decades [2,15–18], allowing to work on several designs and their optimization in order to take advantage of their photonic properties [6,19,20]. On the one hand, not only the use of uniform BGs has grown, but also that of non-uniform designs such us chirped, apodized, phase shifted and tilted structures, which allow controlling their spectral response (bandwidth, smoothness and symmetry) [21,22]. On

the other hand, experimental works regarding AWBGs have also been carried out, in which amplifying [23] and lasing performance [24,25] is achieved, even for multimode and multicore lasers [11,26], showing up the capability and usefulness of AWBGs photonic properties. Nevertheless, the fundamental aspect for a better understanding and optimization of any potential device is that the response of both passive and active behaviors highly depends on the grating parameters, the bulk material where it is written, the fabrication process itself and the operating conditions. Some numerical models have been used in previous works to calculate separately both the passive BG [19,27] and active waveguide responses [28,29]. However, although some theoretical works have been done regarding AWBGs [13,30], a more in-depth study of the fundamental dependences which can drastically modify the AWBG response must be addressed for the design and optimization of these promising structures.

The main goal of this work is to develop a numerical method that allows us to model the AWBG reflective response as a function of its main parameters and working conditions. This will serve for studying the optical power propagation along the AWBG as well as its amplifying and gain properties. In addition, it will be useful as the basis for optimizing the behavior of these structures for promising applications such as monolithic lasing and amplifying reflectors. A theoretical to experimental comparison will be made to ensure the accuracy of the numerical method results and dependences obtained.

The work is organized as follows. Section 2 presents the experimental results obtained with two AWBG structures fabricated and characterized by us. Section 3 describes the numerical method developed to simulate the power propagation along an AWBG. Finally, section 4 presents the simulation results and the discussions.

2. AWBGs EXPERIMENTAL RESULTS

Some uniform AWBGs have been written using femtosecond laser pulses that induce element redistribution within Er^{3+}/Yb^{3+}-codoped phosphate glasses [17]. The experimental writing procedure and the passive Bragg grating significant parameters have been previously optimized [19]. The schematic representation of the experimental set up is shown in Fig. 1.

The laser emits pulses of 350 fs at 1030 nm at a repetition rate of 500 kHz. After crossing a 1.3 mm slit, the beam is focused 150 m underneath the glass surface. First, the guiding core is written within the phosphate glass, with a refractive index n_o = 1.530. A pulse energy of 520 nJ is employed with a scanning sample velocity of 100 µm/s, so that a uniform refractive index change is generated. After the homogeneous waveguide is written, a periodic refractive index perturbation is induced by modulating the 500 kHz pulse train with a 10.3 kHz envelope wave while moving the sample at a scan velocity of 5200 µm/s. As a result, the grating period of this over-imposed index modulation structure is 501.6 nm. Thus, the design Bragg wavelength corresponds to the main amplification wavelength of the Er^{3+} ion (1534 nm). The duty cycle of the envelope wave is 5%, adequately selected from a previous theoretical-to-experimental optimization to maximize the Bragg grating reflectivity [19]. As a consequence, gratings with a passive reflectivity value (hereinafter referred to as R_p) up to $R_p = 0.85$ are produced. Fig. 2 presents the passive spectral reflectivity of three 10 mm long gratings, showing up narrow bandwidths below 1 nm. Their different reflectivity values are due to the different laser pulse

energies (in the range of 700-780 nJ) used in the second scanning process that produces the refractive index perturbations (of the order of Δn = 6$\times$10^{-3}).

In order to study the active behavior, a symmetric bidirectional pump power is injected at both grating ends (pump wavelength: $\lambda = 976$ nm). The light emitted in the counterpropagating direction in a wavelength range around 1534 nm is then registered for several injected pump powers. Results with the $R_p = 0.84$ AWBG are shown in Fig. 3.

As shown in Fig. 3(a), when the pump power employed is lower than 216 mW, a small amplified spontaneous emission (ASE) signal is generated by the AWBG, with the expected maximum peak at around 1534 nm. The higher the pump, the higher the power obtained in the whole spectral response. On the other hand, as shown in Fig. 3(b), when the pump power employed is more than 216 mW, the ASE power drastically increases by four orders of magnitude reaching almost 10 μW, indicating that lasing occurs, but only around the grating reflective peak, with a narrow bandwidth of 1.6 nm due to the BG filtering. The higher the pump, the higher the ASE power, at least in the range employed in our case, limited to 245 mW by our equipment. This behavior has been only observed when the pump power is bidirectionally injected. This measuring procedure has also been carried out in the other two 10 mm gratings before mentioned, with passive reflectivities of $R = 0.73$ and 0.81, showing a similar behavior.

In addition, 5 mm long AWBGs have also been fabricated to check the same dependences. In that case, any significant ASE signal as the one observed in Fig. 3(b) has not been detected regardless of their efficiencies and the pump power injected.

Thus, a significant ASE power is detected in experimental AWBGs, which leads to the laser phenomenon of these structures. However, its performance highly depends on the pumping conditions and characteristic parameters of the Bragg gratings (length and reflective efficiency). The combination of all these conditions determines not only the power values obtained but also whether lasing in the AWBG can be achieved or not. In order to better understand and optimize the behavior of these structures, the AWBGs amplifying response has to be modeled.

3. NUMERICAL METHOD

A numerical program has been implemented in order to simulate the optical power propagation evolution within an active Er^{3+}/Yb^{3+}-codoped integrated waveguide working at the emission spectrum peak wavelength (1534 nm). This theoretical method is an update of the one employed by Benedicto *et al* [29], which showed a good theoretical-to-experimental match with active waveguides. In this work, the Bragg grating consideration has been added to the program to simulate the AWBG reflective behavior.

3.1. Optical power propagation

In order to numerically simulate the active and reflective behavior throughout the AWBG, the grating is divided in N small enough uniform sections (20-30 sections/mm). The propagated power and its derivative are both calculated in each section by using a Runge-Kutta method so that their evolution along the waveguide propagation direction z can be determined. The next equation is calculated by the program in each i-th section:

$$\frac{dP_i(z)}{dz} = \left[A(\eta,\sigma,z) - \alpha + \frac{\ln(t_i)}{\Delta z}\right] P_i(z) \quad (1)$$

Three terms are found within the brackets, which govern the final amplification properties of the AWBG. The first one, $A(\eta,\sigma,z)$, is a function which determines the Er/Yb-codoped waveguide active behavior along the propagation direction z depending on the overlapping factors between the mode intensity and levels population density distributions, η, and on the transition cross sections, σ. More details about this function can be found in [29]. The second term, α, is the medium's power propagation loss coefficient. This coefficient only accounts for the scattering losses, while the absorption cross section losses are already included in the function $A(\eta,\sigma,z)$. Finally, the third term is the main point of this work since it represents the reflective characteristic of the Bragg grating written along the active medium by means of the transmission coefficient, t_i, of each Δz-long section.

These contributions have opposite effects on the propagated power and its derivate: the active term corresponds to the amplification of light power, while the others may reduce it by attenuation or internal reflection respectively. It should be noted that the reflective term contributes negatively to the power derivative in Eq. (1) since the transmission coefficient is lower than one at the wavelengths in which the Bragg grating is working. The contribution of these terms may lead to the amplification and even lasing behavior that are to be studied in this work.

3.2. Iterative calculation

The co- and counterpropagating powers along the AWBG, hereinafter noted by the subscripts R and L (right and left), can be calculated using Eq. (1) by means of an iterative calculation: the active functions mutually depend on the power of both propagation directions and eventually a convergent solution would be obtained. However, a fundamental point must be considered to our AWBG beyond being a simple active medium: the multiple reflections. A fraction of the copropagated power P_R is reflected by every grating section, so that it turns to contribute to the counterpropagated power P_L, and vice versa. For that reason, an additional term must be added to Eq. (1) in both propagating directions:

$$\begin{aligned}\frac{dP_R(z)}{dz} &= \left[A(\eta,\sigma,z) - \alpha + \frac{\ln(t)}{\Delta z}\right] P_R(z) - \frac{\ln(t)}{\Delta z} P_L(z) \\ \frac{dP_L(z)}{dz} &= \left[A(\eta,\sigma,z) - \alpha + \frac{\ln(t)}{\Delta z}\right] P_L(z) - \frac{\ln(t)}{\Delta z} P_R(z)\end{aligned} \quad (2)$$

where it should be noted that the crossed power terms added to consider the mutual reflective properties always contribute positively ($t < 1$), that is to say, they increase the power derivatives. Therefore, both co- and counterpropagating powers are mutually dependent and could lead to amplified multiple reflections under the appropriate AWBG properties and operating conditions. This way, the AWBG may generate an amplified reflected power even to obtain a significant power gain or the lasing phenomenon. In the later equations, the subscript i related to the i-th section has been omitted for the sake of clarity since the gratings studied are uniform perturbation along the propagation axis and therefore the same t_i is obtained for every section).

In order to develop the iterative calculation, boundary conditions must be considered including the injected pump power and signal power (if such is the case) at both grating ends. Once all the specific considerations are implemented, the copropagating power evolution along the z direction is calculated with Eq. (2), considering $P_L(z) = 0$ as starting condition. Then, the counterpropagating power is calculated backwards analogously, using the already saved $P_R(z)$ values. The $P_L(z)$ values are saved for the new iteration, and so on. Using this iterative numerical method, the signal, fluorescence and pump powers can be determined along the AWBG, so that the reflectivity, transmissivity and propagation evolution profile within the grating can be simulated as a function of the integrated AWBG properties and working conditions.

4. SIMULATIONS RESULTS AND DISCUSSION

The aim of this section is to numerically simulate and analyze the main dependences and behaviors that occurs in the AWBGs. In order to do so, several sets of uniform AWBGs have been simulated as a function of the most relevant parameters that affect their response. In addition, the final goal is to compare the numerical results with our experimental AWBGs responses presented in Fig. 3. For that reason, the experimental Er^{3+}/Yb^{3+}-codoped integrated AWBG specifications and working conditions mentioned in Section 2 have been taken into account in the simulations. The rare earth ion concentrations used are 2.4×10^{26} m^{-3} and 5.1×10^{26} m^{-3} for Er^{3+} and Yb^{3+}, respectively, which correspond to the experimental samples employed. A propagation loss coefficient $\alpha = 1.3$ dB/cm ($\lambda = 1535$ nm) has been considered, which represents a typical value for this kind of waveguides [17].

Simulations have been carried out in the 1525–1540 nm range, with a wavelength resolution of 1 nm. The chosen resolution and working range are a compromise between computational time and reliable results. As seen in Fig. 2, the spectral reflectivity of the experimental Bragg grating has a bandwidth below 1 nm, that is to say, lower than the chosen simulation resolution. For that reason, in order to simulate the Bragg grating contribution in this discretized resolution spectrum, the Bragg peak has been simply modeled as a delta function with a transmission coefficient at λ = 1535 nm corresponding to the maximum value of the experimental peak. Although this delta representation is not totally realistic compared to the experimental spectral profile, its effect to the reflective behavior is expected to be similar due to the wavelength resolution employed. In fact, several tests have been done to check that considering small values at both sides of the peak do not represent, by any means, a significant quantitative deviation (at least for the simulations addressed in this work). Thus, the delta function representation of the experimental spectra seems to be reasonable. The transmission coefficient at the rest of the wavelength range has been considered zero, so no reflective effects take place there. Since the AWBG simulated are uniform, the $t(\lambda)$ values are the same for each grating section in the numerical calculations.

In order to study the amplification and gain properties of these AWBGs as well as the power propagation along them, a small 1 μW signal power is injected at the entrance of the waveguide ($z = 0$), which is a value far from the active medium to get saturated.

4.1. Amplification pump power dependence

Simulations of a 10 mm long AWBG have been carried out with different bidirectional pump power values, injected symmetrically at both waveguide ends. The grating simulated in this point has a passive reflectivity $R_p = 0.50$. The signal power propagation results, normalized to the injected signal, are presented in Fig. 4 along the AWBG z-direction.

When no pump is injected, the propagated power rapidly decreases due to absorption, propagation losses and the BG reflections. The penetration length is just about 3-4 mm, so that just a short effective AWBG length is working as the light is lost before propagating through the entire grating. However, when the pump power is injected, the penetration length increases and starts reaching the effects of the pump power injected at the opposite end. As a consequence, the effective working length of the AWBG increases, leading to an increase of the grating reflectivity at its entrance ($z = 0$): from $R_p = 0.50$ to $R = 0.90$ with just 150 mW bidirectional pump. When the pump power is high enough, all the grating can be actively working and an effective gain in the reflected signal power is obtained: $R = 1.24$ with 300 mW pump.

These simulations show how the AWBG response can drastically vary from a small amplification of the reflected signal towards a reflector with significant signal gain when modifying the pump power employed.

4.2. Bragg grating reflective efficiency

The maximum reflectivity of a passive Bragg grating of length L is given by [1]:

$$R_{p,max} = \tanh^2(\kappa L) \tag{3}$$

where the BG coupling coefficient, κ, describes the grating reflective efficiency, and is determined by the grating parameters and the fabrication process [19]. The higher the coupling, or the higher the length, the higher the reflectivity (at least until it saturates according to the $tanh$ function). Nevertheless, an extremely efficient BG would imply negative consequences for the AWBG since the more reflective, the more difficult the power to reach the other AWBG end, so the active reflector would not be optimal. On the other hand, another important consideration on the AWBG length must be taken into account related to subsection 4.1 results: the penetration length of the AWBG is clearly increased by the bidirectional pump power injected. When a long grating is considered, more active medium could be working if the appropriate efficiency and pump power is used to make the propagated power to reach the entire grating. This is the reason why both dependencies are highly intermixed and an in-depth study is fundamental.

In order to delve into these dependencies, four sets of simulations have been carried out with six different AWBG lengths (1.5 to 12.5 mm). Each set corresponds to a different passive BG reflectivity ($R_p = 0.40$ to 0.80), that is to say, in each simulation set the product κL remains constant to get the same passive reflectivity, so the grating coupling is properly adjusted. All the simulations have been done with bidirectional symmetric pump power from 0 to 450 mW. Again, a 1 μW signal power is injected to the grating entrance. Results are shown in Fig. 5.

Fig. 5(a) shows a logical dependence on the grating length: although the BG reflectivity is the same, the longer the grating, the higher the reflectivity when the pump power is injected since more AWBG can be actively working. In addition, according to the results discussed in point 4.1, amplification of the reflected signal is higher when the pump power is increased, and even a $R = 1.75$ is achieved in the best case. However, if the pump power is not high enough, the signal power does not reach all the BG since the pump power injected at the waveguide end is too far out the reach of the signal power. As a consequence, the AWBG does not work efficiently and the active behavior is reduced, so that the reflectivity saturates or even decreases. This trend inversion can be clearly observed with 300 and 150 mW pump power, showing a maximum reflectivity with 10 and 5 mm grating length respectively.

On the other hand, as the BG passive reflectivity is increased, a fundamental result is shown up: the amplification and signal gain are clearly favored, Fig. 5(b). The AWBG enters a regime of amplified multiple reflections: the co- and counterpropagating powers feedback each other thanks to the combination of the AWBG reflective and active properties which confines and amplifies the light power. As a consequence, a high signal gain is obtained. If the BG efficiency increases, this high gain also appears for lower pump power values, Fig. 5(c). It must be noted that in all the simulations in this point a limited number of iterations were permitted to minimize the computational time since only the general dependence is aimed at now. However, when the grating enters this self-powered regime, it is expected that the active medium would eventually be saturated when the signal might reach some mW. Nevertheless, this result is highly important since it represents the first step towards the promising lasing phenomenon.

When the BG passive reflectivity becomes too high, the portion of reflected power in every grating section is excessive, and the previous trend is inverted: the power is extremely reflected by every grating section before being sufficiently amplified. Thus, the amplification properties are then generally reduced, as seen in Fig. 5(d) compared to lower passive BG efficiencies. The reason of this trend inversion is clearly observed in Fig. 6, where the distribution of signal power along the z-direction (normalized to the injected signal) of two 7.5 mm AWBGs with different passive reflectivity is presented. A 450 mW bidirectional pump power is employed in both cases.

The $R_p = 0.50$ AWBG result shows how the power signal is amplified all along the grating, so the whole grating length is actively working. The propagated power is then confined and maximized in the grating center, leading to signal gain: the reflectivity at the grating entrance (z = 0) is then $R = 1.80$. However, the $R_p = 0.80$ AWBG points out how the signal power is mainly confined next to the grating entrance when the BG is too efficient. Thus, the AWBG active properties are not optimized in this case, since the signal does not reach adequately the final region of the grating and so only a fraction of it is working. As a consequence, the signal reflectivity obtained at the grating entrance only reaches $R = 1.17$. For this reason, this AWBG would be equivalent to a shorter one, and so its active response.

As observed in this point, a compromise between both AWBG intrinsic properties and working conditions is a key factor in order to optimize the gain/amplification performance.

4.3. Propagation losses dependence

In the previous points, the reflective and active terms in Eq. (2) have been analyzed, but there is another term which might be also critical to the AWBG performance: the propagation losses. Obviously, the more attenuation, the more difficult for the power to propagate through the grating, so that any amplifying effect of the AWBG would be reduced in that case. This critical dependence is pointed out in Fig. 7, in which a 12.5 mm AWBG has been simulated as a function of the pump power injected. It must be noted that, despite not having been considered in Eq. (3), the passive reflectivity depends on the loss coefficient: the more attenuation, the more power is lost along the grating and therefore the lower the passive reflectivity. In this case, a passive reflectivity $R_p = 0.43$ is simulated with α = 1.3 dB/cm. It should be noted, as mentioned in subsection 3.1, that this attenuation coefficient only accounts for the scattering losses, while those related to the absorption cross sections are already included in the active function in Eq. (1) and (2). Thus, the absorption losses remain constant in all the simulations since the rare-earths cross section are not modified in our work. Again, a 1 µW signal power is injected to the waveguide entrance.

As observed in this result, the medium's propagation loss coefficient is highly critical and the AWBG performance within a small range of typical values for these media might be significantly different. When a 300 mW pump power is used, a $R = 0.96$ amplification turns to $R = 1.45$ when the attenuation goes down from 1.5 to 1.1 dB/cm. In the case of a 450 mW pump power, it turns respectively from $R = 1.20$ to a high off-axis gain value. Therefore, considering this key factor is a must in order to any theoretical-to-experimental comparison.

4.4. Amplified spontaneous emission simulations

As mentioned in Fig. 5 discussions, under some particular values of the grating parameters and pumping conditions, the signal gain starts increasing significantly because the self-powered multiple reflections regime of the AWBG. Thus, when only the pump power is injected without any signal power, the active medium would be expected to generate an amplified spontaneous emission (ASE) signal around the rare-earth most efficient wavelength [28], as observed experimentally in Fig. 3. On the contrary, the propagation loss coefficient is a parameter hard to be controlled in the AWBG fabrication process with a significant contribution to the AWBG response, as seen before.

For those reasons, in order to analyze all these contributions and to simulate our experimental results, several sets of simulations of a 10 mm AWBG with passive reflectivity $R_p = 0.80$ have been carried out as a function of the pump power injected for different propagation losses of the medium. Results of the ASE power at 1534 nm are shown in Fig. 8, compared to the experimental values obtained in Fig. 3(b).

As observed, the values obtained from the simulations reasonably match the experimental results for losses of the order of those typically observed in this type of waveguides. It should be taken into account that the BG writing process might slightly increase the bulk media scattering loss coefficient (typically between 1-1.3 dB/cm [17]) so that a value between 1.30 and 1.43 dB/cm seems to be positively consistent. This represents a very important result which verifies that the simulation method has been adequately developed and set up, but also that the

experimental fabrication process and the AWBG response are correct and coherent, and only a higher pump power would be needed to experimentally obtain a high lasing performance in this case. In fact, this good match indicates that the numerical method could be employed in further works in order to simulate and optimize the AWBG lasing behavior and design.

Finally, regarding the 5 mm AWBG also mentioned in Section 2, as indicated, significant ASE signal was not experimentally detected. Considering the theoretical simulations of a 5 mm AWBG from Fig. 5, it can be seen that the reflectivity does not drastically increase: a significant gain ($R = 1.31$) is detected in the best case, but it should be taken into account that the propagation loss coefficient used in those simulations is α = 1.30 dB/cm, lower than what Fig. 8 results suggest. Therefore, the amplification in 5 mm AWBGs would be even lower, and so, any ASE signal might not be significant enough, matching again the experimental results.

5. CONCLUSIONS

A numerical method has been implemented in this work to simulate the power propagation along an AWBG, which takes into account its reflective and active properties. The simulations carried out have allowed to study and better understand the AWBG response dependences on the most relevant grating parameters, pumping and propagation losses of the waveguide. Results have shown that the optimal values of the main AWBG parameters can maximize its performance as a highly amplified reflectors, which would be quite interesting for its use as mirrors of a laser cavity.

On the other hand, the AWBG spontaneous emission has been theoretically observed within a particular BG design (length and efficiency) and pumping. The propagation losses reveal as a key factor for a future accurate adjustment of the theoretical results to the experimental ones since it can be affected by the AWBG writing process itself. Nevertheless, the simulations carried out match adequately the experimental ASE results within an acceptable losses range, confirming the appropriate development of the numerical method to simulate the AWBG response, but also the correctness and consistency of the AWBG experimental design and fabrication process addressed in this work. These positive results are the basis for further works on the quantitative selection and optimization of the AWBG design as well as for its amplifying and lasing performance.

ACKNOWLEDGEMENTS

This work was partially supported by the grants PID2020-112770RB-C21 and PID2019-108598GB-I00 funded by MCIN/AEI/10.13039/501100011033, and by the Department of Industry and Innovation (Government of Aragón) through the research group Grant E44-20R (cofinanciado con FEDER 2014-2020: Construyendo Europa desde Aragón). S.F. acknowledges the projects CUD-2021_05 and CUD-2023_12 of the Centro Universitario de la Defensa de Zaragoza. M.M. acknowledges the postdoctoral Juan de la Cierva Incorporación grant (IJCI-2017-33317) of the Spanish Ministry of Research and Innovation.

REFERENCES

[1] Kashyap R., "*Fiber Bragg Gratings*", 2nd ed. (Elsevier, 2010).

[2] Ams M., Dekker P., Gross S., and Withford M.J., "*Fabricating waveguide Bragg gratings (WBGs) in bulk materials using ultrashort laser pulses*", Nanophotonics **6** (2017) 743–763.

[3] Kaminow I., Li T., and Willner A.E., "*Optical Fiber Telecommunications Volume VIA, Sixth Edition: Components and Subsystems*", 6th ed. (Academic Press, Inc., 2013).

[4] Idrisov R., Lorenz A., Rothhardt M., and Bartelt H., "*Composed Multicore Fiber Structure for Extended Sensor Multiplexing with Fiber Bragg Gratings*", Sensors **22** (2022) 3837.

[5] Malayappan B., Krishnaswamy N., and Pattnaik P.K., "*Optical MEMS Accelerometer Based on Waveguide Bragg Grating Integrated with Crab-Leg Beam*", in *2020 IEEE SENSORS* (IEEE, 2020), pp. 1–4.

[6] Butt M.A., Kazanskiy N.L., and Khonina S.N., "*Advances in Waveguide Bragg Grating Structures, Platforms, and Applications: An Up-to-Date Appraisal*", Biosensors **12** (2022) 497.

[7] Urban F., Kadlec J., Vlach R., and Kuchta R., "*Design of a Pressure Sensor Based on Optical Fiber Bragg Grating Lateral Deformation*", Sensors **10** (2010) 11212–11225.

[8] Osellame R., Chiodo N., Della Valle G., Cerullo G., Ramponi R., Laporta P., Killi A., Morgner U., and Svelto O., "*Waveguide lasers in the C-band fabricated by laser inscription with a compact femtosecond oscillator*", IEEE J. Sel. Top. Quantum Electron. **12** (2006) 277–285.

[9] del Hoyo J., Moreno-Zarate P., Escalante G., Valles J.A., Fernandez P., and Solis J., "*High-Efficiency Waveguide Optical Amplifiers and Lasers via FS-Laser Induced Local Modification of the Glass Composition*", J. Light. Technol. **35** (2017) 2955–2959.

[10] Turitsyn S.K., Babin S.A., El-Taher A.E., Harper P., Churkin D. V., Kablukov S.I., Ania-Castañón J.D., Karalekas V., and Podivilov E. V., "*Random distributed feedback fibre laser*", Nat. Photonics **4** (2010) 231–235.

[11] Kurkov A.S., Grukh D.A., Medvedkov O.I., Paramonov V.M., Dianov E.M., Yashkov M. V., Vechkanov N.I., and Guryanov A.N., "*Multimode fiber lasers based on Bragg gratings and double-clad Yb-doped fibers*", Laser Phys. Lett. **1** (2004) 473–475.

[12] Carras M., Garcia M., Marcadet X., Parillaud O., De Rossi A., and Bansropun S., "*Top grating index-coupled distributed feedback quantum cascade lasers*", Appl. Phys. Lett. **93** (2008) 011109.

[13] Mozjerin I., Ruschin S., and Hardy A., "*Design of unidirectional erbium-doped waveguide ring laser with asymmetric distributed Bragg grating*", Electron. Lett. **41** (2005) 1119.

[14] Shi W., Veerasubramanian V., Plant D. V., Jaeger N.A.F., and Chrostowski L., "*Silicon photonic Bragg-grating couplers for optical communications*" in *Next-Generation Optical Networks for Data Centers and Short-Reach Links*, Proc. of SPIE Vol. 9010 (2014), p. 90100F.

[15] Choi J., Ramme M., and Richardson M., "*Directly laser-written integrated photonics devices including diffractive optical elements*", Opt. Lasers Eng. **83** (2016) 66–70.

[16] Choudhury D., Macdonald J.R., and Kar A.K., "*Ultrafast laser inscription: perspectives on future integrated applications*", Laser Photon. Rev. **8** (2014) 827–846.

[17] Macias-Montero M., Dias A., Sotillo B., Moreno-Zarate P., Ariza R., Fernandez P., and Solis J., "*Waveguide Tapers Fabrication by Femtosecond Laser Induced Element Redistribution in Glass*", J. Light. Technol. **38** (2020) 6578–6583.

[18] Osellame R., Taccheo S., Marangoni M., Ramponi R., Laporta P., Polli D., De Silvestri S., and Cerullo G., "*Femtosecond writing of active optical waveguides with astigmatically shaped beams*", J. Opt. Soc. Am. B **20** (2003) 1559.

[19] Sanz-Felipe Á., Macias-Montero M., Valles J.A., and Solis J., "*Waveguide Bragg gratings fabrication and optimization as a function of the duty cycle*", in *XII Reunión Española de Optoelectrónica, OPTOEL'21* (2021), pp. 59–64.

[20] del Hoyo J., Vazquez R.M., Sotillo B., Fernandez T.T., Siegel J., Fernández P., Osellame R., and Solis J., "*Control of waveguide properties by tuning femtosecond laser induced compositional changes*", Appl. Phys. Lett. **105** (2014) 131101.

[21] Navruz I. and Altuncu A., "*Design of a chirp fiber Bragg grating for use in wideband dispersion compensation*", in *New Trends in Computer Networks* (Imperial College Press, 2005), pp. 114–123.

[22] Palumbo G., Tosi D., Iadicicco A., and Campopiano S., "*Analysis and Design of Chirped Fiber Bragg Grating for Temperature Sensing for Possible Biomedical Applications*", IEEE Photonics J. **10** (2018) 1-15.

[23] Ennser K., Della Valle G., Ibsen M., Shmulovich J., and Taccheo S., "*Erbium-doped waveguide amplifier for reconfigurable WDM metro networks*", IEEE Photonics Technol. Lett. **17** (2005) 1468–1470.

[24] Das B.K., Ricken R., and Sohler W., "*Integrated optical distributed feedback laser with Ti:Fe:Er:LiNbO3 waveguide*", Appl. Phys. Lett. **82** (2003) 1515–1517.

[25] Panyaev I., Zolotovskii I., and Sannikov D., "*Laser generation and amplification of TE and TM modes in a semiconductor optical GaAs waveguide with distributed feedback generated by a space charge wave*", Opt. Commun. **459** (2020) 125026.

[26] Alon Y., Halstuch A., Sidharthan R., Yoo S., and Ishaaya A.A., "*Femtosecond Bragg grating inscription in an Yb-doped large-mode-area multicore fiber for high-power laser applications*", Opt. Lett. **45** (2020) 4563.

[27] Stathopoulos N.A. and Simos I., "*Modelling of non-uniform and fs-Laser inscribed fibre Bragg gratings*", Opt. Fiber Technol. **70** (2022) 102878.

[28] Valles J.A., Rebolledo M.A., and Cortes J., "*Full Characterization of Packaged Er–Yb-Codoped Phosphate Glass Waveguides*", IEEE J. Quantum Electron. **42** (2006) 152–159.

[29] Benedicto D., Dias A., Martin J., Valles J.-A., and Solis J., "*Characterization of Multicore Integrated Active Waveguides Written in an Er 3+ /Yb 3+ Codoped Phosphate Glass*", J. Light. Technol. **39** (2021) 5061–5068.

[30] Stathopoulos N.A., Savaidis S.P., Simos H., Rangoussi M., and Kervalishvili P., "*Simulation and properties of Erbium-Doped Distributed Bragg Reflectors (ED-DBRs) and Fiber Bragg Gratings (ED-FBGs)*", Opt. Fiber Technol. **19** (2013) 369–377.

FIGURES

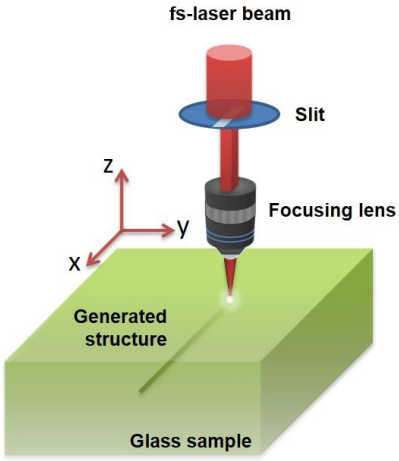

Fig. 1. Schematic representation of the fs-laser induced element redistribution irradiation setup.

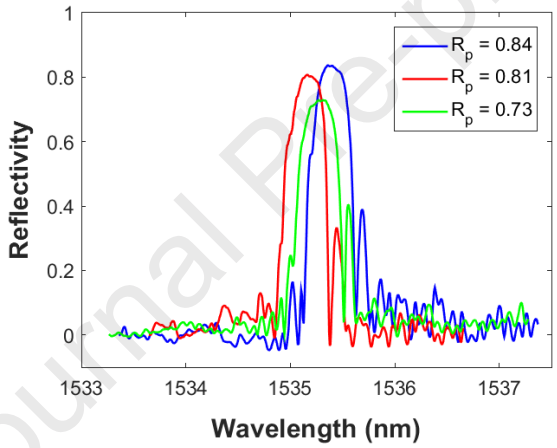

Fig. 2. Spectral reflectivity of three 10 mm long BGs written within the Er/Yb-codoped waveguide. The passive reflectivity R_p around the designed Bragg wavelength is presented.

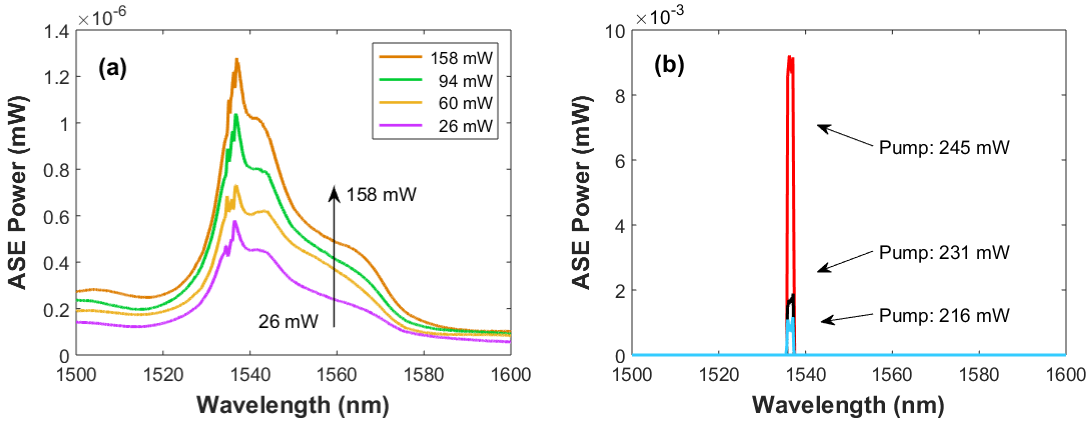

Fig. 3. ASE power spectra obtained with the $R_p = 0.84$ AWBG shown in Fig. 2 when pump power lower (a) and larger (b) than 216 mW is bidirectionally injected.

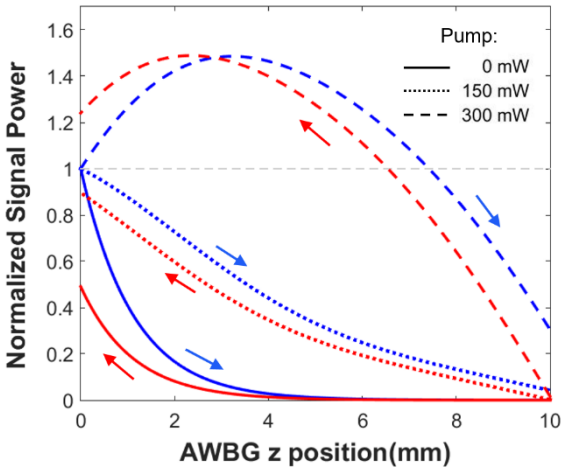

Fig. 4. Normalized signal power along the AWBG propagation direction z as a function of the pump power injected symmetrically. Co- and counterpropagating powers are shown (blue and red respectively) and indicated with the arrows. Signal power is injected at $z = 0$.

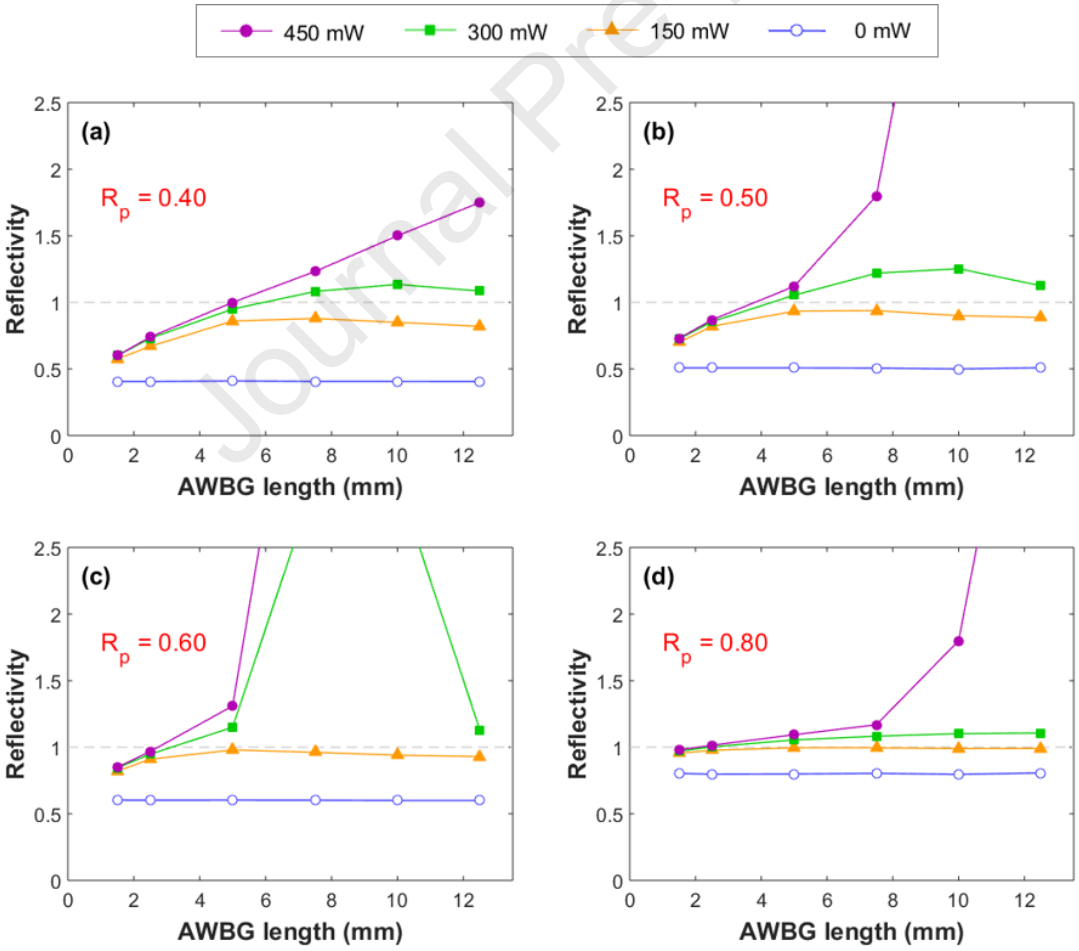

Fig. 5. Simulated AWBGs reflectivities as a function of their length and pump power injected bidirectionally. In each case, the passive reflectivity remains constant by adjusting the coupling coefficient to maintain the product κL constant.

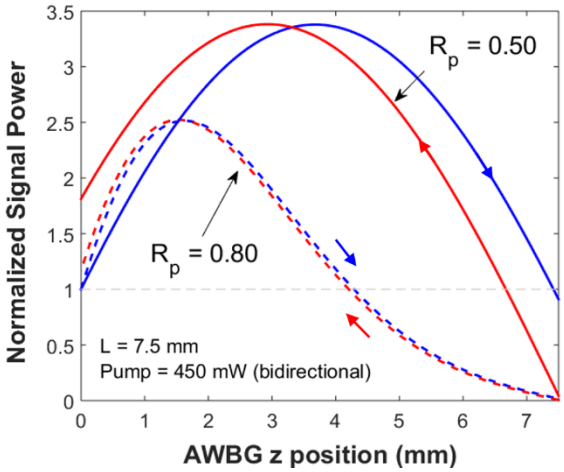

Fig. 6. Distribution of the normalized signal power along the AWBG z-direction of two 7.5 mm gratings simulated with $R_p = 0.50$ (continuous line) and $R_p = 0.80$ (dashed line). Co- and counterpropagating powers are shown (blue and red respectively) and indicated with the arrows. Signal power is injected at z = 0.

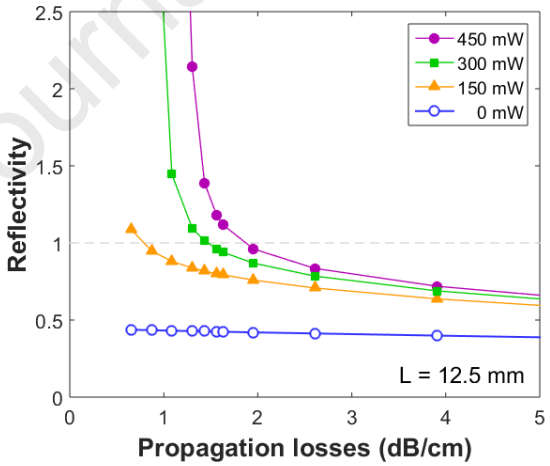

Fig. 7. Reflectivity of a 12.5 mm AWBG as a function on the propagation losses of the media. Four values of the pump power have been employed in the simulations. The passive reflectivity of the grating with α = 1.3 dB/cm is $R_p = 0.43$.

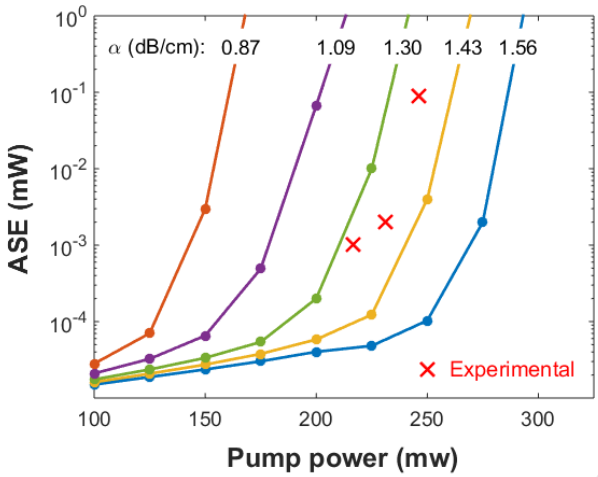

Fig. 8. Amplified spontaneous emission (ASE) power at 1534 nm simulated as a function of the pump power employed in a 10 mm $R_p = 0.80$ AWBG. Curves for several propagation losses coefficients are shown, labeled with the corresponding α. Experimental values from Fig. 3(b) are included (×).

Declaration of interests

☒ The authors declare that they have no known competing financial interests or personal relationships that could have appeared to influence the work reported in this paper.

☐The authors declare the following financial interests/personal relationships which may be considered as potential competing interests: